CrystEngComm

PAPER

View Article Online
View Journal | View Issue

Published on 13 January 2015. Downloaded by National University of Singapore on 7/7/2024 8:04:52 AM.

Cite this: *CrystEngComm*, 2015, **17**, 1833

Size-controlled synthesis of Pd nanosheets for tunable plasmonic properties†

Yi Li, Yucong Yan, Yuheng Li, Hui Zhang,* Dongsheng Li* and Deren Yang

Received 13th October 2014,
Accepted 11th January 2015

DOI: 10.1039/c4ce02062f

www.rsc.org/crystengcomm

Hexagonal Pd nanosheets with extremely thin thickness are synthesized in high yields by reducing the Pd salt precursor in *N*,*N*-dimethylformamide (DMF) containing tungsten hexacarbonyl ($W(CO)_6$), citric acid (CA), and cetyltrimethylammonium bromide (CTAB). During the reaction, $W(CO)_6$ spontaneously decomposes to W particles and CO, serving as reducing and capping agents in the synthesis of Pd nanosheets, respectively. We found that the use of CA and CTAB is both beneficial to promote the formation of hexagonal Pd nanosheets with stacking faults. In addition, the edge length of the Pd nanosheets can be simply tuned by varying the amount of CA fed in the synthesis. Such nanosheets can be further grown by subsequent seeded growth with as-preformed Pd nanosheets as the seeds. The Pd nanosheets with different edge lengths exhibit tunable localized surface plasmon resonance (LSPR) in the range of 820–1067 nm, and thus hold great potential in the field of plasmon-enhanced catalysis.

Introduction

Metal nanocrystals have attracted steadily growing attention from both the scientific and industrial communities because of their widespread use in catalysis, plasmonics, and biological medicine.[1–6] Manipulating their plasmonic properties is particularly critical for achieving advances in many areas, including surface-enhanced Raman scattering, energy harvesting and conversion, sensing, and imaging.[7–13] It is well-known that the plasmonic properties of metal nanocrystals are highly sensitive to their composition, size, and shape.[14–17] In general, coinage metals, such as Au, Ag, and Cu, have been considered as important materials for localized surface plasmon resonance (LSPR) owing to their unique properties that arise from a strong interaction between incident light and free electrons in such metals.[18–20] In addition, there are strong efforts in controlling the size and shape of the metals since these two parameters play a key role in determining their plasmonic properties.[21–24] The last decade has witnessed the successful synthesis of nanocrystals in a rich variety of shapes made of Au, Ag, and Cu, with notable examples including cubes, octahedra, tetrahedra, decahedra, icosahedra, prisms, rods, and high-index faceted nanostructures.[25–29] Of these shapes, prisms with an extremely high degree of anisotropy are a particularly interesting class of structure, which favor a high tunability of their plasmonic properties.[30–32] To this end, many research groups have demonstrated the photochemical or chemical synthesis of the prisms made of Ag and Au for tunable LSPR from visible to near-infrared (NIR) regions by simply varying their edge length, thickness, and snip.[33–37] Despite these enormous successes, exploring a new material system for LSPR applications is still an important and permanent issue that needs to be addressed urgently.

Palladium (Pd) is a key component of many catalysts used in industrial processes and commercial devices.[38] Depending on its dielectric function, however, Pd is not a promising candidate to support LSPR at high intensity.[19] In addition, its LSPR peak is typically located in the ultraviolet spectral range, which makes the LSPR characteristics much more difficult to probe due to the strong absorption of light at these wavelengths by glass vessels and most solvents. Recently, numerous efforts have been employed to tailor the LSPR properties of Pd nanocrystals by controlling their size and shape. For instance, Xia *et al.* found that the LSPR peak of Pd nanocubes could be shifted to the visible region by increasing their sizes to >25 nm.[39] Excavating Pd nanocubes into nanoboxes or nanocages with hollow structures could tune their LSPR peaks from 420 to 510 nm.[40] In addition, decreasing the size of Pd nanocrystals in one dimension to generate triangular or hexagonal plates also red-shifted their LSPR peaks to 520 nm.[41] Overall, it is still very difficult to synthesize Pd nanocrystals with LSPR peaks located in NIR regions, which is very important for biological applications. Recently, Zheng *et al.* have demonstrated a facile synthesis of

State Key Lab of Silicon Materials, Department of Materials Science and Engineering, and Cyrus Tang Center for Sensor Materials and Applications, Zhejiang University, Hangzhou, Zhejiang 310027, PR China.
E-mail: msezhanghui@zjue.edu.cn; Fax: +86 571 87952322; Tel: +86 571 87953190

† Electronic supplementary information (ESI) available. See DOI: 10.1039/c4ce02062f

Published on 13 January 2015. Downloaded by National University of Singapore on 7/7/2024 8:04:52 AM.

hexagonal-shaped Pd nanosheets 1.8 nm in thickness.[42,43] Yang *et al.* have demonstrated the synthesis of Hanoi Tower-like multilayered and three-dimensional Pd nanosheets.[44,45] Both of these two reports inevitably involve the use of very toxic gas (*i.e.*, CO) as reducing and capping agents during the synthesis.

Here, we report a facile approach to the synthesis of Pd nanosheets with controlled edge length in *N*,*N*-dimethylformamide (DMF) containing tungsten hexacarbonyl ($W(CO)_6$), citric acid (CA), and cetyltrimethylammonium bromide (CTAB). By replacing CO with $W(CO)_6$, our strategy for the synthesis of Pd nanosheets can be much more easily implemented in the lab. More importantly, these Pd nanosheets possess smaller edge length (<10 nm) and thinner thickness (*ca.* 1 nm) relative to the previously reported ones.[42] In addition, such Pd nanosheets exhibit the tunable LSPR peaks located in the NIR region with the varied edge length.

Experimental section

Chemicals and materials

Palladium(II) acetylacetonate ($Pd(acac)_2$, 99%), polyvinyl pyrrolidone (PVP, MW = 29 000), and tungsten hexacarbonyl ($W(CO)_6$, 97%) were purchased from Sigma-Aldrich. Citric acid (CA), cetyltrimethylammonium bromide (CTAB), *N*,*N*-dimethylformamide (DMF, AR), ethanol (AR), and acetone (AR) were purchased from Sinopharm Chemical Reagent Co., Ltd. All the chemicals were used as received.

Synthesis of Pd nanosheets with different sizes

In a standard synthesis of Pd nanosheets with an average edge length of 35.8 nm, 16 mg of $Pd(acac)_2$, 10 mg of CA, 60 mg of CTAB, and 30 mg of PVP were dissolved in 10 mL of DMF and stirred for 1 h. The resulting homogeneous orange-red solution was then transferred into a 25 mL flask and 100 mg of $W(CO)_6$ were added into the flask under an Ar atmosphere. Subsequently, the flask was capped and heated at 80 °C for 1 h. After the reaction, the Pd nanosheets were isolated by centrifugation using a sufficient amount of acetone, and then re-dispersed in ethanol. This process was repeated three times. To achieve Pd nanosheets with edge lengths from 24.5 to 15.7, 9.2, and 6.4 nm, the amount of CA fed in the synthesis was increased from 50 to 90, 130, and 170 mg, respectively, with all other parameters being the same as in the standard procedure.

Synthesis of Pd nanosheets by seeded growth

To further enlarge the edge length of Pd nanosheets, seeded growth was employed with as-preformed Pd nanosheets as the seeds. For example, 46.9 nm Pd nanosheets were synthesized by mixing 13.1 mmol of as-preformed Pd nanosheets with an average edge length of 35.8 nm, 8 mg of $Pd(acac)_2$, and 50 mg of PVP in 10 mL of DMF in a 25 mL flask. Subsequently, 50 mg of $W(CO)_6$ were added into the flask under an Ar atmosphere. The flask was capped and heated at 60 °C for 4 h. After the reaction, the Pd nanosheets were isolated by centrifugation using a sufficient amount of acetone, and then re-dispersed in ethanol. This process was repeated three times. The 59.2 nm Pd nanosheets were synthesized by using 46.9 nm Pd nanosheets as the seeds, with all other parameters being the same as in the aforementioned procedure.

Morphological, structural, and elemental characterization

Transmission electron microscopy (TEM) images were taken using a HITACHI HT-7700 microscope operated at 100 kV. High-resolution TEM (HRTEM) was performed using a FEI Tecnai G2 F20 microscope operated at 200 kV. Energy dispersive X-ray spectroscopy (EDX) was performed using a Titan G2 80-200 ChemiSTEM equipped with a Super-X EDX detector system. Extinction spectra were taken on a Hitachi U-4100 spectrophotometer at a scan speed of 300 nm min^{-1} by using ethanol as the solvent.

Results and discussion

Fig. 1 shows morphological and structural characterization of the Pd nanosheets prepared using the standard procedure. From TEM images in the figure, a and b, most of the nanocrystals have a hexagon profile with a little proportion of rhombus shape due to the projection along the <111> zone axis. It is clear that each hexagonal nanosheet consists of six regular triangles, while the rhombus shape is formed by two regular triangles sharing an edge. The average edge length of the Pd nanosheets was measured to be *ca.* 35.8 nm (see the inset of Fig. 1a). These data were obtained from 200 nanocrystals randomly selected from TEM images. Due to the extremely thin thickness, the Pd nanosheets show weak TEM

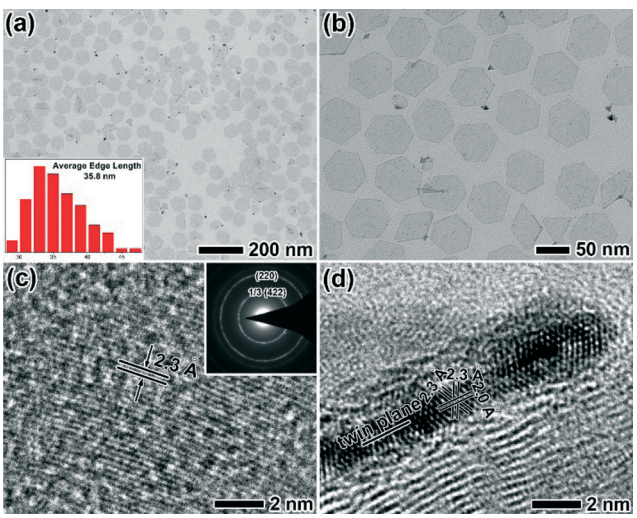

Fig. 1 (a, b) TEM images of Pd nanosheets obtained using the standard procedure. The inset in (a) shows the edge length distribution of the Pd nanosheets. (c, d) HRTEM images of an individual nanosheet laid flat and stood vertically on the TEM grid, respectively. The inset in (c) corresponds to the selected area electron diffraction (SAED) pattern.

 This journal is © The Royal Society of Chemistry 2015

Published on 13 January 2015. Downloaded by National University of Singapore on 7/7/2024 8:04:52 AM.

contrast when they lay flat on a copper grid. Fig. 1c shows a HRTEM image of an individual Pd nanosheet that lays flat on the surface of carbon films. The fringes with a lattice spacing of 2.3 Å can be indexed to the {111} planes of Pd with a fcc structure. To measure the thickness of the Pd nanosheets, carbon nanotubes were used as the support to allow the attachment of the nanosheets vertically to the outer surface of the nanotubes. From the TEM image in Fig. S1,† the thickness of these Pd nanosheets was measured to be *ca.* 1.1 nm. Fig. 1d shows a typical HRTEM image of the side surface of an individual nanosheet that vertically stands on the TEM grid. The fringes with lattice spacings of 2.0 and 2.3 Å can be indexed to the Pd{200} and {111}, respectively. Careful observation reveals that there are {111} stacking faults parallel to their flat faces in such a nanosheet. The extremely thin thickness makes our Pd nanosheets really unstable under the high strong electron beam of TEM. So we could not get a clear electron diffraction spot but the 1/3(422) diffraction ring was observed (see the inset of Fig. 1c). Based on the TEM and HRTEM characterization, we can conclude that such nanosheets are similar to the previously reported nanosheets,[42] but have the extremely thin thickness. EDX equipped on TEM (see Fig. S2a† for the spectrum) shows that there are three elements in the sample: Pd, C, and Cu. Obviously, Pd came from the Pd nanosheets, while C and Cu originated from the carbon-coated copper grid. EDX mapping of single nanosheet in the inset of Fig. S2a† shows that only the Pd element is uniformly distributed in the nanosheet and almost no impurities such as W can be detected from the sample. This result indicates that the nanosheets are only made of Pd.

We can control the size of Pd nanosheets by varying the amounts of CA fed in the synthesis. Fig. 2 shows TEM images of the Pd nanosheets prepared using the standard procedure, except for the different amounts of CA. From these TEM images, the average edge length of the Pd nanosheets decreased from 25 to 6 nm with increasing amounts of CA from 50 to 170 mg. The size variation of Pd nanosheets can be attributed to different amounts of nuclei formed in the initial stage associated with the reduction rate. According to the experimental observation (Fig. S3†), the color of the solution gradually darkened after the reaction with the increase in the amount of CA, indicating the accelerated reduction rate and thus the increased nuclei. This demonstration is also supported by the seeded growth of the larger Pd nanosheets using as-performed Pd nanosheets with relatively smaller edge length as the seeds. As shown in Fig. 3, the Pd nanosheets with average edge lengths of 46.9 and 59.2 nm were generated by the aforementioned seeded growth. The thickness of these Pd nanosheets with different average edge lengths was measured through TEM analyses with these samples being attached vertically to the carbon nanotube (see Fig. S4†). All of these Pd nanosheets exhibited similar thickness with a value of *ca.* 1 nm. As such, the edge length of the Pd nanosheets can be tuned from 6.4 to 59.2 nm by varying the amount of CA in combination with the subsequent seed-mediated growth while keeping their thickness unchanged.

In order to decipher the growth mechanism of the Pd nanosheets, a series of samples obtained at different reaction times were collected for TEM observation. From Fig. 4a (t = 2.5 min), a large number of small nanosheets with an edge length of *ca.* 10 nm were initially generated. As the reaction proceeded (Fig. 4, b–d), these small nanosheets then served as the seeds and gradually enlarged through lateral growth. From the viewpoint of crystallography, such nanostructures generally evolve from the seeds with stacking faults by maximizing the surface coverage with {111} facets under thermodynamic control. To achieve such nanosheets with extremely thin thickness, the use of $W(CO)_6$, CA, and CTAB is all indispensable. In the absence of $W(CO)_6$, the color of the solution

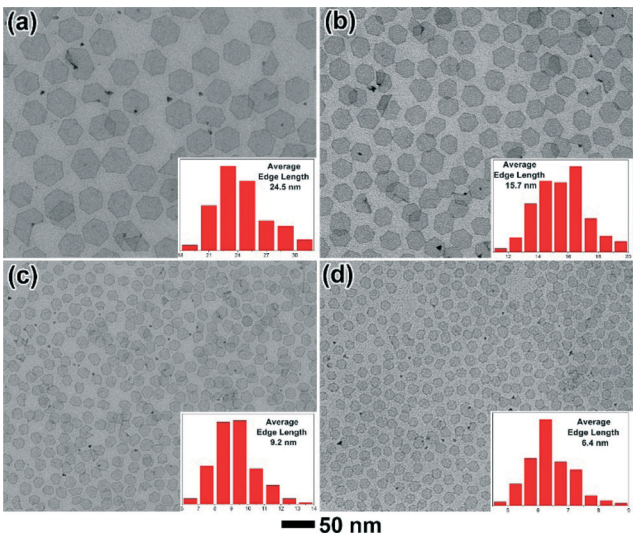

Fig. 2 TEM images of Pd nanosheets prepared using the standard procedure, except for different amounts of citric acid fed in the synthesis: (a) 50, (b) 90, (c) 130, and (d) 170 mg. The insets show the corresponding edge length distributions of Pd nanosheets.

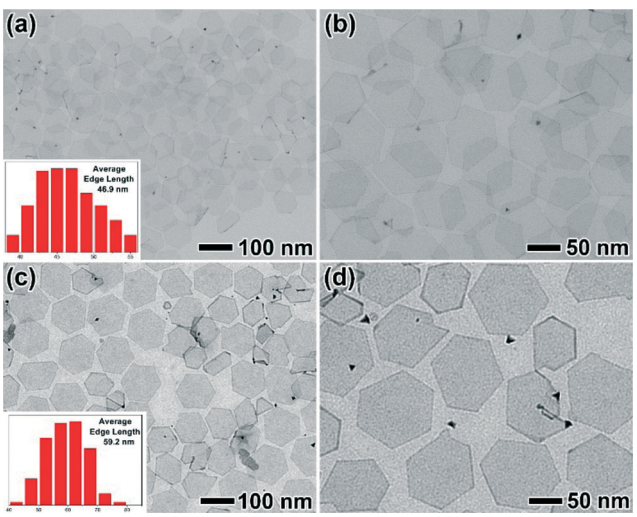

Fig. 3 TEM images of Pd nanosheets prepared by seed-mediated growth with (a, b) 35.8 nm Pd nanosheets and (c, d) 46.9 nm Pd nanosheets as the seeds. The insets in (a) and (c) show the corresponding edge length distributions.

Published on 13 January 2015. Downloaded by National University of Singapore on 7/7/2024 8:04:52 AM.

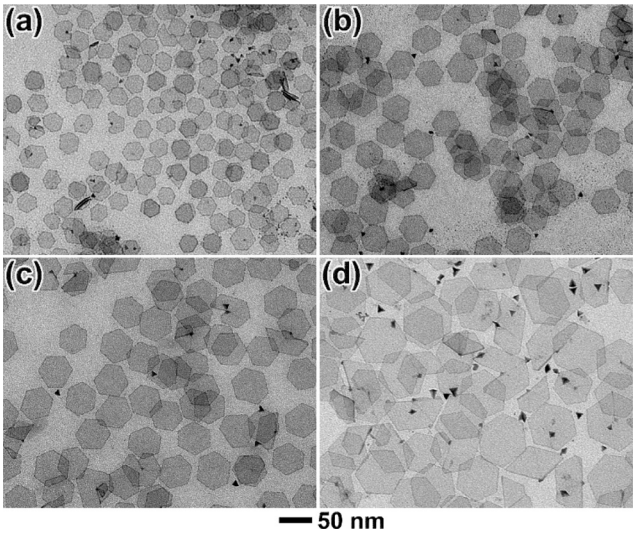

Fig. 4 TEM images of Pd nanocrystals prepared using the standard procedure, except for different reaction times: (a) 2.5, (b) 10, (c) 20, and (d) 40 min.

only turned from paint yellow to rose pink at 80 °C for 1 h and no solid product was generated (Fig. S5a†), indicating that $W(CO)_6$ served as a reducing agent in this synthesis. According to a previous report,[46] $W(CO)_6$ decomposed instantaneously during the reaction, resulting in the spontaneous formation of W particles and CO. The as-formed W particles could help reduce $Pd(acac)_2$ to Pd atoms (or seeds) rapidly in the early stage of the nucleation. The peaks of W^{4+}, W^{5+}, and W^{6+} were observed in the X-ray photoelectron spectrum (XPS) of the reaction residue in the standard procedure (Fig. S6†), indicating that W^0 was oxidized and thus acted as a reducing agent in the reaction. Obviously, CO arising from the decomposition of $W(CO)_6$ served as a capping agent to facilitate the formation of the Pd nanosheet due to the extremely strong adsorption on the {111} facets.[42] This demonstration was also supported by the formation of the Pd nanosheets when $W(CO)_6$ was replaced with $Cr(CO)_6$ as the reducing and capping agents (Fig. S5b†). Obviously, the amount of $W(CO)_6$ is of great importance to the formation of Pd nanosheets, as shown in Fig. S7.† When the amount of $W(CO)_6$ is decreased to 10 mg, Pd nanosheets are still generated but co-existed with a large number of Pd tetrahedra (Fig. S7a†), indicating that CO is not sufficient in the formation of Pd nanosheets. Further studies show that this kind of nanosheet is not stable when aged for 3–4 days due to insufficient CO to stabilize them (Fig. S7b†). Increasing the amount of $W(CO)_6$ from 50 to 200 mg shows no difference either in edge length or thickness of the nanosheets (Fig. S7, c–f†).

In addition to $W(CO)_6$, CA and CTAB also play a key role in promoting the formation of the Pd nanosheets. To investigate the action of CA and CTAB, a set of control experiments were carried out. Two flasks were loaded with 10 mL of DMF and 100 mg of $W(CO)_6$ under Ar protection with one flask having additional 10 mg of CA and 60 mg of CTAB. As shown in Fig. S8, a and d,† $W(CO)_6$ did not dissolved in DMF in both flasks at room temperature. After heating at 80 °C, $W(CO)_6$ quickly dissolved and formed as a clear and transparent solution in the absence of CA and CTAB (Fig. S8b†). When the flask was cooled down back to room temperature, many $W(CO)_6$ were separated out of the solution (Fig. S8c†). This result indicates that $W(CO)_6$ decomposed very slowly at 80 °C. In the presence of CA and CTAB, however, the color of the solution turned to dark green immediately (Fig. S8e†), indicating the quick decomposition of $W(CO)_6$ at 80 °C. This demonstration was also supported by the no obvious change in color after cooling down to room temperature (Fig. S8f†). XPS analysis of the reaction residue (Fig. S6†) further confirmed the above-mentioned demonstration. As a result, the presence of CA and CTAB can promote the decomposition of $W(CO)_6$ at a relatively low temperature. Based on these results, it was not hard to explain that why only little Pd tetrahedron was generated when only $W(CO)_6$ was used in the reaction system (Fig. S9a†), while the nanosheets were formed in the presence of CA and/or CTAB (Fig. S9, b and c†). It is well-known that CA can block oxidative etching and promote the formation of stacking faults due to the strong binding of this species to the Pd surface[47] and thus dramatically decrease the percentage of single crystal nuclei. However, it is still inevitable to find a small amount of Pd tetrahedra with exposed {111} planes in this synthesis (Fig. S9f†). Br^- ions derived from CTAB can form a stable complex of $PdBr_4^{2-}$ with Pd^{2+} ions, which was found to facilitate the formation of twinned structures.[48] As such, the reactions only in the presence of both CTAB and CA yielded high-quality hexagon-shaped Pd nanosheets. In addition, the use of CA can have a strong complex with the reduced species of W^{6+} ions and thus accelerate the reduction reaction.[49] As such, the edge length of the Pd nanosheets decreased with increasing amount of CA due to the more rapid nucleation. The use of CTAB is essential to maintain the hexagonal shape of the Pd nanosheets by manipulating the lateral growth with its strong binding to the {100} planes.[42] When CTAB was replaced with CTAC, the proportion of the nanosheets obviously decreased and the size of the nanosheet is not uniform (Fig. S9e†), indicating that Br^- ions are also better in the formation of twinned structures and size control than Cl^- ions. In the absence of PVP, most of the products are aggregated, indicating that PVP serves as a stabilizing agent (Fig. S9d†).

The LSPR properties of the Pd nanosheets with different average edge lengths were then evaluated by UV-vis-NIR extinction spectra, as shown in Fig. 5. As observed from Fig. 5a, it is clear that each sample exhibits only one broad peak in the extinction spectra with a wavelength range of 400–1400 nm. According to the previous result,[50] these single LSPR peaks can be assigned to the in-plane dipole resonance of the Pd hexagonal nanosheets. No other high-order multipole LSPR of such nanosheets can be resolved in the measurements. By increasing the edge lengths of the nanosheets with a similar thickness, their LSPR peaks gradually red-shift from 820 to 1067 nm due to the enhanced aspect ratio for the two-dimensional anisotropy (Fig. 5b), which was

 This journal is © The Royal Society of Chemistry 2015

Published on 13 January 2015. Downloaded by National University of Singapore on 7/7/2024 8:04:52 AM.

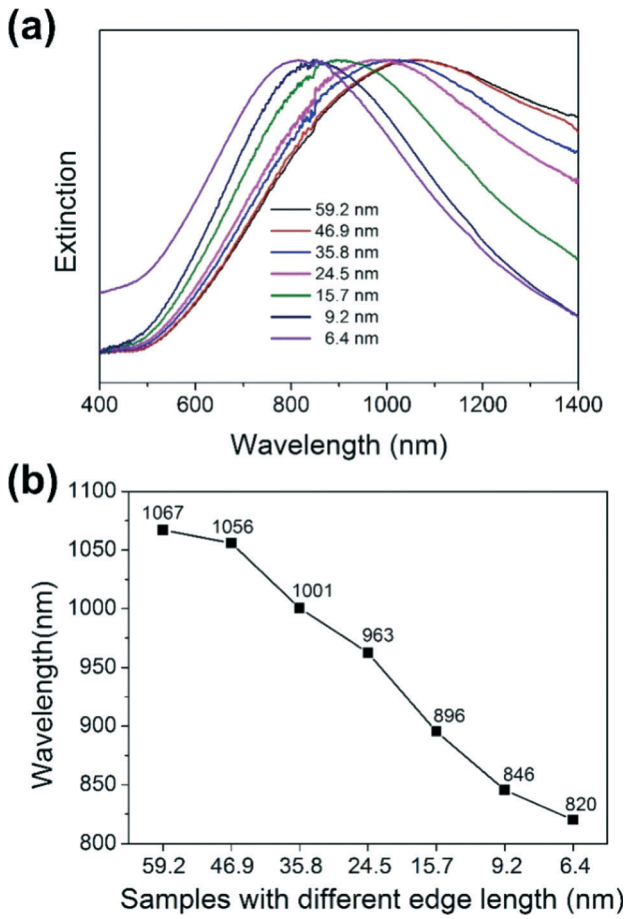

Fig. 5 (a) UV-vis-NIR extinction spectra of the Pd nanosheets with different average edge lengths. (b) Plots of LSPR peaks with average edge length of the Pd nanosheets.

consistent with the previous result.[42] Owing to their unique plasmonic properties, the Pd nanosheets are expected to serve as promising catalysts with the enhanced catalytic performance promoted by LSPR.[51]

Conclusions

We have developed a facile approach to the synthesis of Pd hexagonal nanosheets with extremely thin thickness. The use of $W(CO)_6$, CA, and CTAB was found to play key roles in facilitating the formation of such nanosheets. The edge length of Pd nanosheets can be simply tuned from 6.4 to 59.2 nm by varying the amount of CA fed in the synthesis, together with the subsequent seeded-growth process. The Pd nanosheets with different average edge lengths show the tunable LSPR properties in the NIR region, which might be interesting in the field of plasmon-enhanced catalysis.

Acknowledgements

This work was supported by NSFC (no. 51372222) and the Fundamental Research Funds for the Central Universities (no. 2014FZA4007).

Notes and references

1 M. Debe, *Nature*, 2012, **486**, 43–51.
2 Y. Wu, D. Wang and Y. Li, *Chem. Soc. Rev.*, 2014, **43**, 2112–2124.
3 O. Hess, J. Pendry, S. Maier, R. Oulton, J. Hamm and K. Tsakmakidis, *Nat. Mater.*, 2012, **11**, 573–584.
4 S. Lal, J. Hafner, N. Halas, S. Link and P. Nordlander, *Acc. Chem. Res.*, 2012, **45**, 1887–1895.
5 L. Dykman and N. Khlebtsov, *Chem. Soc. Rev.*, 2012, **41**, 2256–2282.
6 E. Dreaden, A. Alkilany, X. Huang, C. Murphy and M. El-Sayed, *Chem. Soc. Rev.*, 2012, **41**, 2740–2779.
7 J. Li, Y. Huang, Y. Ding, Z. Yang, S. Li, X. Zhou, F. Fan, W. Zhang, Z. Zhou, D. Wu, B. Ren, Z. Wang and Z. Tian, *Nature*, 2010, **464**, 392–395.
8 L. Tong, T. Zhu and Z. Liu, *Chem. Soc. Rev.*, 2011, **40**, 1296–1304.
9 G. Baffou and R. Quidant, *Chem. Soc. Rev.*, 2014, **43**, 3898–3907.
10 S. Boriskina, H. Ghasemi and G. Chen, *Mater. Today*, 2013, **16**, 375–386.
11 K. Saha, S. Agasti, C. Kim, X. Li and V. Rotello, *Chem. Rev.*, 2012, **112**, 2739–2779.
12 L. Rodríguez-Lorenzo, R. de la Rica, R. Álvarez-Puebla, L. Liz-Marzán and M. Stevens, *Nat. Mater.*, 2012, **11**, 604–607.
13 X. Qian, X. Peng, D. Ansari, Q. Yin-Goen, G. Chen, D. Shin, L. Yang, A. Young, M. Wang and S. Nie, *Nat. Biotechnol.*, 2008, **26**, 83–90.
14 N. Motl, A. Smith, C. Desantis and S. Skrabalak, *Chem. Soc. Rev.*, 2014, **43**, 3823–3834.
15 J. Nelayah, M. Kociak, O. Stephan, F. Abajo, M. Tencé, L. Henrard, D. Taverna, I. Pastoriza-Santos, L. Liz-Marzán and C. Colliex, *Nat. Phys.*, 2007, **3**, 348–353.
16 Y. Xia and N. Halas, *MRS Bull.*, 2005, **30**, 338–348.
17 K. Kelly, E. Coronado, L. Zhao and G. Schatz, *J. Phys. Chem. B*, 2003, **107**, 668–677.
18 H. Chen, L. Shao, Q. Li and J. Wang, *Chem. Soc. Rev.*, 2013, **42**, 2679–2724.
19 M. Rycenga, C. Cobley, J. Zeng, W. Li, C. Moran, Q. Zhang, D. Qin and Y. Xia, *Chem. Rev.*, 2011, **111**, 3669–3712.
20 N. Halas, S. Lal, W. Chang, S. Link and P. Nordlander, *Chem. Rev.*, 2011, **111**, 3913–3961.
21 M. Huang and P. Lin, *Adv. Funct. Mater.*, 2012, **22**, 14–24.
22 T. Ming, W. Feng, Q. Tang, F. Wang, L. Sun, J. Wang and C. Yan, *J. Am. Chem. Soc.*, 2009, **131**, 16350–16351.
23 Y. Ma, Q. Kuang, Z. Jiang, Z. Xie, R. Huang and L. Zheng, *Angew. Chem., Int. Ed.*, 2008, **47**, 8901–8904.
24 B. Wiley, S. Im, Z. Li, J. McLellan, A. Siekkinen and Y. Xia, *J. Phys. Chem. B*, 2006, **110**, 15666–15675.
25 Y. Xia, Y. Xiong, B. Lim and S. Skrabalak, *Angew. Chem., Int. Ed.*, 2009, **48**, 60–103.
26 A. Tao, S. Habas and P. Yang, *Small*, 2008, **4**, 310–325.
27 Z. Quan, Y. Wang and J. Fang, *Acc. Chem. Res.*, 2013, **46**, 191–202.

Published on 13 January 2015. Downloaded by National University of Singapore on 7/7/2024 8:04:52 AM.

28 M. Langille, M. Personick and C. Mirkin, *Angew. Chem., Int. Ed.*, 2013, **52**, 13910–13940.
29 M. Grzelczak, J. Pérez-Juste, P. Mulvaney and L. Liz-Marzán, *Chem. Soc. Rev.*, 2008, **37**, 1783–1791.
30 J. Millstone, S. Hurst, G. Métraux, J. Cutler and C. Mirkin, *Small*, 2009, **5**, 646–664.
31 L. Sherry, R. Jin, C. Mirkin, G. Schatz and R. Van Duyne, *Nano Lett.*, 2006, **6**, 2060–2065.
32 Q. Zhang, Y. Wang, J. Li, R. Iurilli, S. Xie and D. Qin, *ACS Appl. Mater. Interfaces*, 2013, **5**, 6333–6345.
33 R. Jin, Y. Cao, C. Mirkin, K. Kelly, G. Schatz and J. Zheng, *Science*, 2001, **294**, 1901–1903.
34 R. Jin, Y. Cao, E. Hao, G. Métraux, G. Schatz and C. Mirkin, *Nature*, 2003, **425**, 487–490.
35 Q. Zhang, N. Li, J. Goebl, Z. Lu and Y. Yin, *J. Am. Chem. Soc.*, 2011, **133**, 18931–18939.
36 J. Zeng, X. Xia, M. Rycenga, P. Henneghan, Q. Li and Y. Xia, *Angew. Chem., Int. Ed.*, 2011, **50**, 244–249.
37 J. Millstone, G. Metraux and C. Mirkin, *Adv. Funct. Mater.*, 2006, **16**, 1209–1214.
38 A. Roucoux, J. Schulz and H. Patin, *Chem. Rev.*, 2002, **102**, 3757–3778.
39 Y. Xiong, J. McLellan, J. Chen, Y. Yin, Z. Li and Y. Xia, *J. Am. Chem. Soc.*, 2005, **127**, 17118–17127.
40 Y. Xiong, J. Chen, B. Wiley, Y. Xia, Y. Yin and Z. Li, *Nano Lett.*, 2005, **5**, 1237–1242.
41 Y. Xiong, B. Wiley, J. Chen, Z. Li, Y. Yin and Y. Xia, *Angew. Chem., Int. Ed.*, 2005, **44**, 7913–7917.
42 X. Huang, S. Tang, X. Mu, Y. Dai, G. Chen, Z. Zhou, F. Ruan, Z. Yang and N. Zheng, *Nat. Nanotechnol.*, 2011, **6**, 28–32.
43 H. Li, G. Chen, H. Yang, X. Wang, J. Liang, P. Liu, M. Chen and N. Zheng, *Angew. Chem., Int. Ed.*, 2013, **52**, 8368–8372.
44 X. Yin, X. Liu, Y. Pan, K. Walsh and H. Yang, *Nano Lett.*, 2014, **14**, 7188–7194.
45 P. Tin, X. Yin, K. S. Kwok and H. Yang, *Nano Lett.*, 2014, **10**, 5953–5959.
46 J. Zhang and J. Fang, *J. Am. Chem. Soc.*, 2009, **131**, 18543–18547.
47 Y. Xiong, J. McLellan, Y. Yin and Y. Xia, *Angew. Chem., Int. Ed.*, 2007, **46**, 790–794.
48 Y. Xiong, H. Cai, Y. Yin and X. Xia, *Chem. Phys. Lett.*, 2007, **440**, 273–278.
49 J. Cruywagen, L. Kruger and E. Rohwer, *J. Chem. Soc., Dalton Trans.*, 1991, 1727–1731.
50 E. Kooij, W. Ahmed, H. Zandvliet and B. Poelsema, *J. Phys. Chem. C*, 2011, **115**, 10321–10332.
51 K. Fuku, R. Hayashi, S. Takakura, T. Kamegawa, K. Mori and H. Yamashita, *Angew. Chem., Int. Ed.*, 2013, **52**, 7446–7450.

 This journal is © The Royal Society of Chemistry 2015